Mon. Not. R. Astron. Soc. **397,** 913–924 (2009) doi:10.1111/j.1365-2966.2009.14990.x

Relativistic models of magnetars: the twisted torus magnetic field configuration

R. Ciolfi,[1] V. Ferrari,[1⋆] L. Gualtieri[1] and J. A. Pons[2]

[1]*Dipartimento di Fisica 'G.Marconi', Sapienza Università di Roma and Sezione INFN ROMA1, 00185 Roma, Italy*
[2]*Departament de Física Aplicada, Universitat d'Alacant, 03080 Alacant, Spain*

Accepted 2009 April 29. Received 2009 April 28; in original form 2009 March 3

ABSTRACT

We find general relativistic solutions of equilibrium magnetic field configurations in magnetars, extending previous results of Colaiuda et al. Our method is based on the solution of the relativistic Grad–Shafranov equation, to which Maxwell's equations can be reduced. We obtain equilibrium solutions with the toroidal magnetic field component confined into a finite region inside the star, and the poloidal component extending to the exterior. These so-called twisted torus configurations have been found to be the final outcome of dynamical simulations in the framework of Newtonian gravity, and appear to be more stable than other configurations. The solutions include higher-order multipoles, which are coupled to the dominant dipolar field. We use arguments of minimal energy to constrain the ratio of the toroidal to the poloidal field.

Key words: stars: magnetic fields – stars: neutron.

1 INTRODUCTION

In this paper, we construct models of non-rotating, strongly magnetized neutron stars, or *magnetars* (Duncan & Thompson 1992), in general relativity. We extend our previous work (Colaiuda et al. 2008) based on a formalism developed in Konno, Obata & Kojima (1999) and Ioka & Sasaki (2004), including the toroidal field in a *twisted torus* configuration. The extension to this field geometry is accomplished with an appropriate choice of the function which determines, point by point, the ratio between the toroidal and poloidal components of the magnetic field. The non-linear relation among the functions defining the toroidal and poloidal fields naturally leads to couplings between different multipoles, thus making inadequate the one multipole solution which is usually assumed.

A motivation to find consistent equilibrium solutions in general relativity with this particular geometry comes from recent progresses in numerical magnetohydrodynamic (MHD) simulations, that have made possible to study the dynamics and the stability of magnetic stars. By following the time evolution of generic initial configurations, in the framework of Newtonian gravity and using polytropic EOS, Braithwaite & Spruit (2004) and Braithwaite & Nordlund (2006) (see also Braithwaite & Spruit 2006) have found magnetic field configurations, which are stable on time-scales much longer than the Alfvèn time: they decay only due to finite resistivity. These configurations are roughly axisymmetric; the poloidal field extends throughout the entire star and to the exterior, while the toroidal field is confined in a torus-shaped region inside the star, where the field lines are closed. These configurations were named *twisted torus*. Furthermore, Yoshida, Yoshida & Eriguchi (2006) have shown that such configurations are not significantly affected by rotation; Geppert & Rheinhardt (2006) studied the dependence of magnetostatic equilibrium configurations on the rotational velocity and on the initial angle between rotation and magnetic axis, finding hints for the existence of a unique stable dipolar magnetostatic configuration, independent of the initial field geometry.

We must remark that this particular field geometry resulting from dynamical simulations is obtained by assuming that outside the star there is vacuum; consequently, outside the star electric currents are forbidden and the magnetic field can only be poloidal. This implies that the toroidal field cannot extend to the exterior and that the field lines which cross the surface are purely poloidal, whereas the field lines confined inside the star can maintain a mixed (poloidal and toroidal) structure. This configurations appear to be stable on dynamical time-scales, probably due to magnetic helicity conservation, which requires the persistence of a toroidal component of the field. Note, however, that different solutions including a magnetosphere may be possible. In this case, the toroidal field could also extend to the external region leading to a twisted magnetosphere (Lyutikov 2006; Pavan et al. 2009).

In our perturbative approach, there is a free parameter which represents the ratio between the toroidal and the poloidal components of the magnetic field. We estimate the value of this parameter, by identifying the configuration of minimal energy at fixed magnetic helicity. We also mention that in our configurations the external field has mainly a dipole structure, with small corrections from higher multipoles. Furthermore, confirming a previous suggestion by Prendergast (1956), the toroidal and poloidal fields have amplitudes of the same order of magnitude, whereas the energy associated to the toroidal field is an order of magnitude smaller than that of the

⋆E-mail: valeria.ferrari@roma1.infn.it

poloidal field, since the former is confined in a relatively small region. Similar configurations have been found in Newtonian models including rotation, in Yoshida & Eriguchi (2006) and Yoshida et al. (2006).

In this paper, we consider non-rotating stars because observed magnetars have a very slow rotation rate, although high rotation rates may occur in the early stages of their evolution.

The structure of the paper is as follows. The model is presented in Section 2. In Section 3, we discuss a configuration with purely dipolar magnetic field, neglecting the couplings with higher multipoles. In Section 4, we include the $l = 1$ and 2 field components; Section 5 accounts for the general case, including all multipoles and their couplings. In Section 6, we compute the total energy and the magnetic helicity, and estimate the parameter ζ_0 which determines the ratio between toroidal and poloidal fields by energy minimization; we also compute the magnetic energy, and compare the contributions of the poloidal and toroidal fields for different values of ζ_0. In Section 7, we discuss the results and draw the conclusions.

2 BASIC EQUATIONS AND FORMALISM

We assume that the (non-rotating) magnetized star is stationary and axisymmetric. We further assume that the magnetic field acts as a perturbation of a spherically symmetric background describing a spherical star. The magnetized fluid is described within the framework of ideal MHD, in which the effects of finite electrical conductivity are neglected. Rigorously speaking, this approximation is only valid while the crust is still completely liquid and the core matter has not yet performed the phase transition to the superfluid state, which is expected to occur at most a few hours after birth (see e.g. section 5.1 in Aguilera, Pons & Miralles 2008 and references therein). The onset of superfluidity and/or crystallization limits the period during which magnetostatic equilibrium can be established. Both the melting temperature and the critical temperature of transition to the superfluid state are between 10^9 and 10^{10} K, and a typical neutron star quickly cools down below this temperature in a few hours. However, since the characteristic Alfvén time is of the order of $\tau_{\rm A} \approx 0.01$–10 s, depending on the background field strength, there is ample time for the magnetized fluid to reach a stable state, as shown in Braithwaite & Nordlund (2006), while the state of matter is still liquid. After the crust is formed, the magnetic field is frozen in, and it only evolves on a much longer time-scale due to ohmic dissipation or, in some case, due to the Hall drift (Pons & Geppert 2007). Therefore, it is reasonable to expect that the MHD equilibrium configurations set within the first day after formation will fix the magnetic field geometry for a long time.

Here, we first summarize the basic equations of ideal MHD in the framework of general relativity and then introduce the perturbative approach. Next, we obtain the form of the electromagnetic potential in the case of twisted torus configurations, and derive the relativistic Grad–Shafranov (GS) equation. We use spherical coordinates, $x^\mu = (t, x^a, \phi)$, where $x^a = (r, \theta)$. A stationary axisymmetric space–time admits two killing vectors, $\eta = \partial/\partial t$ and $\xi = \partial/\partial\phi$, and with our coordinate choice all quantities (including the components of the metric tensor $\boldsymbol{g}_{\mu\nu}$) are independent of t and ϕ.

2.1 Equations of ideal MHD in general relativity

According to a comoving observer with four-velocity u^μ, the stress–energy tensor of a perfect fluid with an electromagnetic field is

$$\boldsymbol{T}^{\mu\nu} = \boldsymbol{T}^{\mu\nu}_{\rm fluid} + \boldsymbol{T}^{\mu\nu}_{\rm em}, \tag{1}$$

where

$$\boldsymbol{T}^{\mu\nu}_{\rm fluid} = (\rho + P)u^\mu u^\nu + P g^{\mu\nu}, \tag{2}$$

$$\boldsymbol{T}^{\mu\nu}_{\rm em} = \frac{1}{4\pi}\left[\left(u^\mu u^\nu + \frac{1}{2}g^{\mu\nu}\right)B^2 - B^\mu B^\nu\right]. \tag{3}$$

As usual, Euler's equations are found by projecting the equation $\boldsymbol{T}^{\mu\nu}_{\ ;\nu} = 0$ orthogonally to u^μ

$$(\rho + P)a_\mu + P_{,\mu} + u_\mu u^\nu P_{,\nu} - f_\mu = 0, \tag{4}$$

where $f_\mu \equiv \boldsymbol{F}_{\mu\nu}\, J^\nu$ is the Lorentz force and $a_\mu = u^\nu u_{\mu;\nu}$. Here, $\boldsymbol{F}_{\mu\nu} = \partial_\nu A_\mu - \partial_\mu A_\nu$ is the Maxwell tensor, in terms of which the electric and magnetic fields can be defined as

$$E_\mu \equiv \boldsymbol{F}_{\mu\nu}u^\nu, \quad B_\alpha \equiv \frac{1}{2}\epsilon_{\alpha\beta\gamma\delta}\, u^\beta F^{\gamma\delta}. \tag{5}$$

The basic equations of ideal, general relativistic MHD are then: (i) the continuity equation $(nu^\mu)_{;\mu} = 0$; (ii) Maxwell's equations $\boldsymbol{F}^{\mu\nu}_{\ ;\nu} = 4\pi J^\mu$; (iii) the condition of a vanishing electric field in the comoving frame $E_\mu = \boldsymbol{F}_{\mu\nu}u^\nu = 0$ and (iv) Euler's equations (4).

2.2 The perturbative approach and the form of the electromagnetic potential

We treat the magnetic field as an axisymmetric perturbation of a spherically symmetric background and seek for stationary solutions. The background metric is

$$\mathrm{d}s^2 = -\mathrm{e}^{\nu(r)}\,\mathrm{d}t^2 + \mathrm{e}^{\lambda(r)}\,\mathrm{d}r^2 + r^2(\mathrm{d}\theta^2 + \sin^2\theta\,\mathrm{d}\phi^2), \tag{6}$$

where $\nu(r)$, $\mu(r)$ are solution of the unperturbed Einstein equations for assigned equations of state. The unperturbed four-velocity is $u^\mu = (\mathrm{e}^{-\nu/2}, 0, 0, 0)$. To model the unperturbed neutron star, we use the equation of state (EOS) of Akmal, Pandharipande and Ravenhall called APR2 (Akmal, Pandharipande & Ravenhall 1998), with a standard EOS for the stellar crust (see Benhar, Ferrari & Gualtieri 2004), which results in a neutron star of mass $M = 1.4\,\mathrm{M}_\odot$ and radius $R = 11.58$ km. We remark that our EOS accounts for the density–pressure relation in the crustal region, but not for its elastic properties. Our equations apply to a star where the solid crust has not formed yet, or to configurations with a relaxed crust where elasticity is irrelevant.

It can be shown (see e.g. Colaiuda et al. 2008) that $(\boldsymbol{F}_{\mu\nu}, A_\mu, J^\mu)$ are of the order of $O(B)$, and the perturbations $(\delta u^\mu, \delta\rho, \delta P, \delta n, \delta\boldsymbol{g}_{\mu\nu}, \delta\boldsymbol{G}_{\mu\nu}, \delta\boldsymbol{T}_{\mu\nu})$ are of the order of $O(B^2)$. Therefore, at first order in B the magnetic field is coupled only to the unperturbed background metric (6), whereas the deformation of the stellar structure induced by the magnetic field, which we do not consider in this paper, appears at the order of $O(B^2)$. Furthermore, $(B^t, A_t, J^t, F_{t\nu}) = O(B^3)$ and $(f_t, f_\phi) = O(B^4)$. Note that in the GS equation, which we solve to the order of $O(B)$, the metric perturbations do not appear; thus, to find the magnetic field configurations we do not need to solve Einstein's equations. In Section 6 and Appendix B, we will solve some components of Einstein's equations, in order to evaluate the total energy of the system.

With these assumptions, the potential A_μ, at $O(B)$, has the form $A_\mu(r, \theta) = (0, A_r, A_\theta, A_\phi)$. With an appropriate gauge choice, we can impose $A_\theta = 0$ and write the potential as

$$A_\mu = \left(0, \mathrm{e}^{\frac{\lambda-\nu}{2}}\,\Sigma, 0, \psi\right), \tag{7}$$

where the components of A_μ are expressed in terms of two unknown functions, $\Sigma(r, \theta)$ and $\psi(r, \theta)$.

A further simplification of A_μ is possible by exploiting the fact that $f_\phi = -\psi_{,r}J^r - \psi_{,\theta}J^\theta = O(B^4)$. Using Maxwell's equations and neglecting higher-order terms, we find

$$\tilde{\psi}_{,\theta}\psi_{,r} = \tilde{\psi}_{,r}\psi_{,\theta}, \tag{8}$$

where $\tilde{\psi} \equiv \sin\theta\, \Sigma_{,\theta}$. This result implies $\tilde{\psi} = \tilde{\psi}(\psi)$ and allows us to write

$$\sin\theta\, \Sigma_{,\theta} = \zeta(\psi)\psi\,, \tag{9}$$

where $\zeta(\psi)$ is a function of ψ of the order of $O(1)$.

The function ζ represents the ratio between the toroidal and poloidal components of the magnetic field; different choices of this function lead to qualitatively different field configurations. The simplest case is $\zeta =$ constant (Ioka & Sasaki 2004; Colaiuda et al. 2008; Haskell et al. 2008), but with this choice [like with other simple choices of $\zeta(\psi)$] the field lines of the toroidal field reach the exterior of the star, where there is vacuum. However, the magnetic field in vacuum can only be poloidal (see e.g. Colaiuda et al. 2008), thus this solution presents an inconsistency. To avoid this inconsistency, one should consider a non-vacuum exterior, i.e. a magnetosphere, but modelling a neutron star magnetosphere is a quite difficult task, especially in general relativity. An alternative choice is to assume that the magnetic field is entirely confined inside the star (Ioka & Sasaki 2004; Haskell et al. 2008), but in this way the parameter ζ must assume particular values; or, one can instead accept that the toroidal field has a discontinuity at the stellar surface, vanishing in the exterior (Colaiuda et al. 2008); in this way, the entire range of ζ can be studied, but the discontinuity in the field will, for consistence, imply the existence of surface currents.

A different choice is made in this paper, where we assume that the toroidal field is confined in a toroidal region inside the neutron star, such that its field lines never cross the stellar surface, as in the twisted torus configuration. As mentioned in Section 1, Newtonian numerical simulations (Braithwaite & Spruit 2004; Braithwaite & Nordlund 2006; Braithwaite & Spruit 2006) suggest that these configurations are indeed a quite generic outcome of the evolution of strongly magnetized stars.

The twisted torus configuration can be obtained by choosing the following form of the function ζ:

$$\zeta(\psi) = \zeta_0 \left[|\psi/\bar{\psi}| - 1\right] \Theta(|\psi/\bar{\psi}| - 1). \tag{10}$$

A similar choice has been made, in a Newtonian framework, in Yoshida et al. (2006). In equation (10), ζ_0 is a constant of the order of $O(1)$; $\bar{\psi}$ is a constant of the order of $O(B)$: it is the value of ψ at the boundary of the toroidal region where the toroidal field is confined (this boundary is tangent to the stellar surface); finally, $\Theta(|\psi/\bar{\psi}| - 1)$ is the usual Heaviside function. With this choice, the function ζ vanishes at the stellar surface, where $r = R$, and the magnetic field

$$B^\mu = \left[0, \quad \frac{\mathrm{e}^{-\lambda/2}}{r^2\sin\theta}\psi_{,\theta}, \quad -\frac{\mathrm{e}^{-\lambda/2}}{r^2\sin\theta}\psi_{,r}\ , \right.$$
$$\left. -\frac{\mathrm{e}^{-\nu/2}\zeta_0\psi\left(|\psi/\bar{\psi}| - 1\right)}{r^2\sin^2\theta}\,\Theta(|\psi/\bar{\psi}| - 1)\right] \tag{11}$$

has no discontinuities.

2.3 The relativistic Grad–Shafranov equation

The GS equation, which allows us to determine the magnetic field configuration, can be derived from the ϕ-component of Maxwell's equations

$$J_\phi = -\frac{\mathrm{e}^{-\lambda}}{4\pi}\left(\psi_{,rr} + \frac{\nu_{,r} - \lambda_{,r}}{2}\psi_{,r}\right) - \frac{1}{4\pi r^2}\left(\psi_{,\theta\theta} - \cot\theta\psi_{,\theta}\right) \tag{12}$$

and from the a-components of Euler's equations (4), as follows. Euler's equations give

$$f_a = (\rho + P)a_a + P_{,a} + u_a u^\nu P_{,\nu}$$
$$= (\rho + P)\left(\frac{\nu}{2} - \mathrm{e}^{\nu/2}\delta u^t\right)_{,a} + P_{,a} + O(B^4). \tag{13}$$

For barotropic EOS $P = P(\rho)$, the first principle of thermodynamics allows us to write

$$P_{,a} = (\rho + P)\left(\ln\frac{\rho + P}{n}\right)_{,a}, \tag{14}$$

then (13) yields

$$f_a = (\rho + P)\chi_{,a}, \tag{15}$$

where $\chi = \chi(r, \theta)$. On the other hand, the a components of the Lorentz force $f_\mu = \boldsymbol{F}_{\mu\nu}J^\nu$ can be written as (see Colaiuda et al. 2008)

$$f_a = \frac{\psi_{,a}}{r^2\sin^2\theta}\tilde{J}_\phi, \tag{16}$$

where, in this case,

$$\tilde{J}_\phi = J_\phi - \frac{\mathrm{e}^{-\nu}\zeta_0^2}{4\pi}(\psi - 3\psi|\psi/\bar{\psi}| + 2\psi^3/\bar{\psi}^2)\Theta(|\psi/\bar{\psi}| - 1)\ .$$

Therefore,

$$\frac{\psi_{,a}}{r^2\sin^2\theta}\tilde{J}_\phi = (\rho + P)\chi_{,a}\,. \tag{17}$$

From $\chi_{,r\theta} - \chi_{,\theta r} = 0$, it follows that

$$\psi_{,r}\left[\frac{\tilde{J}_\phi}{(\rho + P)r^2\sin^2\theta}\right]_{,\theta} - \psi_{,\theta}\left[\frac{\tilde{J}_\phi}{(\rho + P)r^2\sin^2\theta}\right]_{,r} = 0,$$

which implies

$$\left[\frac{\tilde{J}_\phi}{(\rho + P)r^2\sin^2\theta}\right] = F(\psi) = c_0 + c_1\psi + O(B^2), \tag{18}$$

with c_0, c_1 constants of the order of $O(B)$, $O(1)$, respectively. Hence, J_ϕ turns out to be

$$J_\phi = \frac{\mathrm{e}^{-\nu}\zeta_0^2}{4\pi}(\psi - 3\psi|\psi/\bar{\psi}| + 2\psi^3/\bar{\psi}^2)\Theta(|\psi/\bar{\psi}| - 1)$$
$$+ (\rho + P)r^2\sin^2\theta\,(c_0 + c_1\psi). \tag{19}$$

From equations (12) and (19), the relativistic GS equation at first order in B is finally obtained:

$$-\frac{\mathrm{e}^{-\lambda}}{4\pi}\left(\psi_{,rr} + \frac{\nu_{,r} - \lambda_{,r}}{2}\psi_{,r}\right) - \frac{1}{4\pi r^2}\left(\psi_{,\theta\theta} - \cot\theta\psi_{,\theta}\right)$$
$$-\frac{\mathrm{e}^{-\nu}\zeta_0^2}{4\pi}\left(\psi - 3\psi|\psi/\bar{\psi}| + 2\psi^3/\bar{\psi}^2\right)\Theta(|\psi/\bar{\psi}| - 1)$$
$$= (\rho + P)r^2\sin^2\theta\,(c_0 + c_1\psi). \tag{20}$$

If we now define $\psi(r, \theta) \equiv \sin\theta a(r, \theta)_{,\theta}$ and expand the function $a(r, \theta)$ in Legendre polynomials

$$a(r, \theta) = \sum_{l=1}^{\infty} a_l(r)P_l(\cos\theta), \tag{21}$$

the GS equation rewrites as

$$-\frac{\sin\theta}{4\pi}\sum_{l=1}^{\infty} P_{l,\theta}\left[\mathrm{e}^{-\lambda}a_l'' + \mathrm{e}^{-\lambda}\frac{\nu'-\lambda'}{2}a_l' - \frac{l(l+1)}{r^2}a_l\right]$$
$$-\frac{\mathrm{e}^{-\nu}}{4\pi}\,\Theta\left(\left|\frac{1}{\bar{\psi}}\sum_{l=1}^{\infty} a_l P_{l,\theta}\sin\theta\right| - 1\right)\,\zeta_0^2\left[\sum_{l=1}^{\infty} a_l P_{l,\theta}\sin\theta\right.$$
$$-\frac{3}{|\bar{\psi}|}\left(\sum_{l,l'=1}^{\infty} a_l P_{l,\theta}\sin\theta\,|a_{l'}P_{l',\theta}\sin\theta|\right)$$
$$\left.+\frac{2}{\bar{\psi}^2}\left(\sum_{l,l',l''=1}^{\infty} a_l a_{l'} a_{l''} P_{l,\theta}P_{l',\theta}P_{l'',\theta}\sin^3\theta\right)\right]$$
$$=(\rho+P)r^2\sin^2\theta\left(c_0 + c_1\sum_{l=1}^{\infty} a_l P_{l,\theta}\sin\theta\right). \qquad (22)$$

Here and in the following, we denote with primes the differentiation with respect to r.

Finally, projecting equation (22) on to the different harmonic components, we obtain a system of coupled ordinary differential equations for the functions $a_l(r)$. The projection is performed using the property

$$\frac{2l'+1}{2l'(l'+1)}\int_0^{\pi} P_{l,\theta}P_{l',\theta}\sin\theta\,\mathrm{d}\theta = \delta_{ll'}. \qquad (23)$$

If we consider the contribution of n different harmonics, we need to solve a system of n coupled equations, obtained from (22), for the n functions $a_l(r)$.

2.4 Boundary conditions

The functions $a_l(r)$ must have a regular behaviour at the origin; by taking the limit $r \to 0$ of the GS equation, one can find

$$a_l(r\to 0) = \alpha_l r^{l+1}, \qquad (24)$$

where α_l are arbitrary constants to be fixed.

Outside the star, where there is vacuum and the field is purely poloidal, equations (22) decouple, and can be solved analytically for each value of l. The solution can be expressed in terms of the generalized hypergeometric functions $[F([l_1, l_2], [l_3], z)]$, also known as Barnes' extended hypergeometric functions, as follows:

$$a_l = A_1 r^{-l} F([l, l+2], [2+2l], z) + A_2 r^{l+1} F([1-l, -1-l], [-2l], z). \qquad (25)$$

where $z = 2M/r$ and A_1 and A_2 are arbitrary integration constants, which must be fixed according to the values of the magnetic multipole moments. Regularity of the external solution at $r = \infty$ requires $A_2 = 0$ for all multipoles. For example, for $l = 1, 2, 3$ we have

$$a_1 \propto r^2\left[\ln(1-z) + z + \frac{z^2}{2}\right],$$
$$a_2 \propto r^3\left[(4-3z)\ln(1-z) + 4z - z^2 - \tfrac{z^3}{6}\right],$$
$$a_3 \propto r^4\left[(15-20z+6z^2)\ln(1-z) + 15z - \frac{25z^2}{2} + z^3 + \frac{z^4}{12}\right]. \qquad (26)$$

At the stellar surface, we require the field to be continuous. This condition is satisfied if a_l and a'_l are continuous. For practical purposes, the boundary conditions at $r = R$ can be written as

$$a_l' = -\frac{l}{R} f_l a_l, \qquad (27)$$

where f_l is a relativistic factor which only depends on the star compactness $2M/R$ (in the Newtonian limit all $f_l = 1$), and can be numerically evaluated with the help of any algebraic manipulator. For our model ($2M/R = 0.357$), the values of f_l for the first five multipoles are 1.338, 1.339, 1.315, 1.301 and 1.292, respectively.

In general, there are $n + 2$ arbitrary constants to be fixed: the n constants α_l, associated to the condition (24), c_0 and c_1. Thus, we need to impose $n + 2$ constraints, of which $n + 1$ are determined by the boundary conditions. n conditions are provided by equation (27), i.e. by imposing continuity in $r = R$ of the ratios a_l'/a_l. The overall normalization of the field gives another condition, which is fixed by imposing that the value of the $l = 1$ contribution at the pole is $B_{\rm pole} = 10^{15}$ G [this corresponds to set $a_1(R) = 1.93 \times 10^{-3}$ km]. The reason for this choice is that the surface value of the magnetic field is usually inferred from observations by applying the spin-down formula, and assuming a purely dipolar external field; for magnetars, the value of B estimated in this way is $\sim 10^{14}-10^{15}$ G. The remaining condition will be imposed as follows.

In the case of a purely dipolar field ($l = 1$), we will assume $c_1 = 0$. In the general multipolar case, we choose to impose that the external contribution of all the $l > 1$ harmonics, i.e. $\sum_{l>1} a_l(R)^2$, is minimum.

3 THE CASE OF PURELY DIPOLAR FIELD

We begin discussing the simplest case of a purely dipolar configuration, in which all couplings with higher-order multipoles are neglected in equation (22) ($a_{l>1} = 0$). In this case, for any assigned value of ζ_0 there exists an infinite set of solutions, each corresponding to a value of c_1; these solutions describe qualitatively similar magnetic field configurations.

However, when higher-order harmonics are taken into account, as we will see in the next section, the picture changes. For instance, when $\zeta_0 = 0$ and the $l = 1, 2$ harmonic components are included, the equations for a_1 and a_2 decouple: the equation for a_1 is the same as in the purely dipolar case, but a solution for a_2 satisfying the appropriate boundary conditions exists only for a unique value of c_1. Therefore, in the general case c_1 is not a truly free parameter (this is true also for $\zeta_0 \neq 0$), and the fact that in the purely dipolar case it looks as such, is an artefact of the truncation of the $l > 1$ multipoles. In order to provide a mathematically simple example, which will be useful to understand the structure of the twisted torus configurations, in this section we will consider the simplest case $c_1 = 0$.

By projecting equation (22) on to the $l = 1$ harmonic, and neglecting all contributions from $l > 1$ terms, we find

$$\frac{1}{4\pi}\left(\mathrm{e}^{-\lambda}a_1'' + \mathrm{e}^{-\lambda}\frac{\nu'-\lambda'}{2}a_1' - \frac{2}{r^2}a_1\right)$$
$$-\frac{\mathrm{e}^{-\nu}}{4\pi}\int_0^{\pi}(3/4)\,\Theta\left(\left|\frac{-a_1\sin^2\theta}{\bar{\psi}}\right| - 1\right)$$
$$\times\,\zeta_0^2\left(-a_1 + 3a_1\left|\frac{-a_1\sin^2\theta}{\bar{\psi}}\right| - 2a_1^3\sin^4\theta/\bar{\psi}^2\right)\sin^3\theta\,\mathrm{d}\theta$$
$$=(3/4)\int_0^{\pi} c_0(\rho+P)r^2\sin^3\theta\,\mathrm{d}\theta = c_0(\rho+P)r^2. \qquad (28)$$

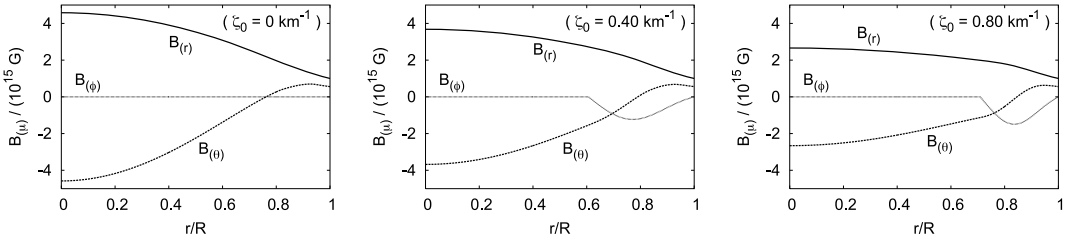

Figure 1. The profiles of the tetrad components of the magnetic field [$B_{(r)}(\theta = 0)$, $B_{(\theta)}(\theta = \pi/2)$, $B_{(\phi)}(\theta = \pi/2)$] are shown for the purely dipolar case with $\zeta_0 = 0$, 0.40 and 0.80 km^{-1}.

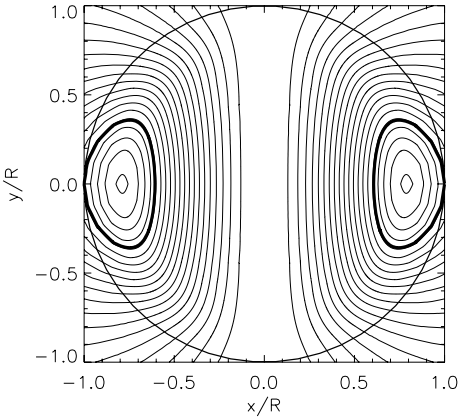

Figure 2. The projection of the field lines in the meridional plane are shown for the purely dipolar case with $\zeta_0 = 0.40\,\mathrm{km}^{-1}$. The toroidal field is confined within the marked region.

The tetrad components of the magnetic field (i.e. the components measured by a locally inertial observer) are

$$
\begin{aligned}
B_{(r)} &= \frac{\psi_{,\theta}}{r^2 \sin\theta},\\
B_{(\theta)} &= -\frac{\mathrm{e}^{-\lambda/2}}{r\sin\theta}\psi_{,r},\\
B_{(\phi)} &= -\frac{\mathrm{e}^{-\nu/2}\zeta_0\psi\left(|\psi/\bar{\psi}|-1\right)}{r\sin\theta}\Theta(|\psi/\bar{\psi}|-1),
\end{aligned}
\tag{29}
$$

where $\psi = -a_1 \sin^2\theta$.

The profiles of the tetrad components of the field inside the star are plotted in Fig. 1 for increasing values of ζ_0; $B_{(r)}$ is evaluated in $(\theta = 0)$ and $B_{(\theta)}$, $B_{(\phi)}$ in $(\theta = \pi/2)$. In Fig. 2, we show the projection of the field lines in the meridional plane, for $\zeta_0 = 0.40\,\mathrm{km}^{-1}$. Figs 1 and 2 show that the toroidal field $B_{(\phi)}$ is confined within a torus-shaped region; its amplitude ranges from zero, at the border of the region, to a maximum, close to its centre. At the stellar surface and in the exterior, B^{ϕ} vanishes, showing that there is no discontinuity in the toroidal field. The panels of Fig. 1 show the field profiles for different values of ζ_0: larger values of ζ_0 correspond to a toroidal field with increasing amplitude, confined in an increasingly narrow region close to the stellar surface, while the amplitude of the poloidal components [$B_{(r)}$, $B_{(\theta)}$] decreases. We remark that this implies that inside the star we cannot have a twisted torus configuration where the toroidal component dominates with respect to the poloidal one: if $|B_{(\phi)}|$ becomes larger with respect to $|B_{(r)}|$ and $|B_{(\theta)}|$, the domain where it is non-vanishing shrinks.

4 THE CASE WITH $l = 1$ AND 2 MULTIPOLES

We now proceed with our investigation by considering the $l = 1$ and 2 contributions, and setting $a_{l>2} = 0$. The projection of the GS equation (22) on to the harmonics $l = 1$ and 2 gives the following coupled equations:

$$
\begin{aligned}
&\frac{1}{4\pi}\left(\mathrm{e}^{-\lambda}a_1'' + \mathrm{e}^{-\lambda}\frac{\nu'-\lambda'}{2}a_1' - \frac{2}{r^2}a_1\right)\\
&\quad -\frac{\mathrm{e}^{-\nu}}{4\pi}\int_0^{\pi}(3/4)\,\Theta\left(\left|\frac{-a_1 - 3a_2\cos\theta}{\bar{\psi}}\sin^2\theta\right| - 1\right)\\
&\quad \times\zeta_0^2\Bigg[-a_1 - 3a_2\cos\theta + 3(a_1 + 3a_2\cos\theta)\\
&\quad \times\left|\frac{-a_1 - 3a_2\cos\theta}{\bar{\psi}}\sin^2\theta\right| + 2\sin^4\theta\Big(-a_1^3 - 9a_1^2a_2\cos\theta\\
&\quad -27a_1a_2^2\cos^2\theta - 27a_2^3\cos^3\theta\Big)/\bar{\psi}^2\Bigg]\sin^3\theta\,\mathrm{d}\theta\\
&\quad = (\rho + P)r^2\left(c_0 - \frac{4}{5}c_1a_1\right),
\end{aligned}
\tag{30}
$$

$$
\begin{aligned}
&\frac{1}{4\pi}\left(\mathrm{e}^{-\lambda}a_2'' + \mathrm{e}^{-\lambda}\frac{\nu'-\lambda'}{2}a_2' - \frac{6}{r^2}a_2\right)\\
&\quad +\frac{\mathrm{e}^{-\nu}}{4\pi}\int_0^{\pi}(5/12)\,\Theta\left(\left|\frac{-a_1 - 3a_2\cos\theta}{\bar{\psi}}\sin^2\theta\right| - 1\right)\\
&\quad \times\zeta_0^2\Bigg[-a_1 - 3a_2\cos\theta + 3(a_1 + 3a_2\cos\theta)\\
&\quad \times\left|\frac{-a_1 - 3a_2\cos\theta}{\bar{\psi}}\sin^2\theta\right| + 2\sin^4\theta\Big(-a_1^3 - 9a_1^2a_2\cos\theta\\
&\quad -27a_1a_2^2\cos^2\theta - 27a_2^3\cos^3\theta\Big)/\bar{\psi}^2\Bigg](-3\cos\theta\sin^3\theta)\,\mathrm{d}\theta\\
&\quad = -\frac{4}{7}(\rho + P)r^2c_1a_2.
\end{aligned}
\tag{31}
$$

We integrate this system by imposing the boundary conditions discussed above, i.e. a regular behaviour at the origin (equation 24) and continuity at the surface of a_1, a_1', a_2, a_2' with the analytical external solutions given by (26).

Let us first consider the simple case $\zeta_0 = 0$. Equations (30) and (31) decouple, and become

$$
\begin{aligned}
&\mathrm{e}^{-\lambda}a_1'' + \mathrm{e}^{-\lambda}\frac{\nu'-\lambda'}{2}a_1' - \frac{2}{r^2}a_1\\
&\quad = 4\pi(\rho + p)r^2\left[c_0 - \frac{4}{5}c_1a_1\right],\\
&\mathrm{e}^{-\lambda}a_2'' + \mathrm{e}^{-\lambda}\frac{\nu'-\lambda'}{2}a_2' - \frac{6}{r^2}a_2\\
&\quad = -\frac{16\pi}{7}(\rho + p)r^2c_1a_2\,.
\end{aligned}
\tag{32}
$$

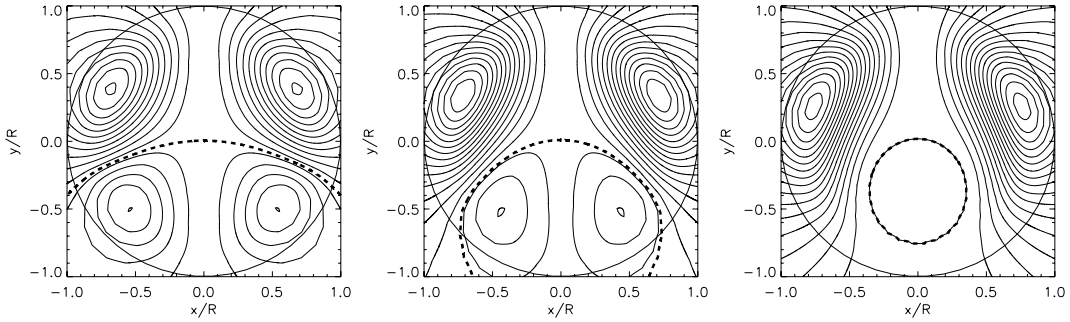

Figure 3. The projection of the field lines in the meridional plane are shown for $\zeta_0 = 0\,\mathrm{km}^{-1}$ and $a_2(R)/a_1(R) = 1, 1/2, 1/4$, respectively, and for $a_{l>2} = 0$. The dashed line corresponds to $\psi = 0$.

There are four constants to fix (α_1, α_2, c_0, c_1) and three conditions: $a_1(R) = 1.93 \times 10^{-3}$ km (normalization) and the ratios $a'_1(R)/a_1(R)$ and $a'_2(R)/a_2(R)$ from the matching with the exterior solutions; thus, we need an additional requirement. We remark that we cannot impose $c_1 = 0$ as in the purely dipolar case, because the ratio $a_2'(R)/a_2(R)$ depends only on c_1, and the matching with the exterior solution is possible only for a particular value of c_1, i.e. $c_1 = 0.84\,\mathrm{km}^{-2}$.

If we impose that $|a_2(R)|$ is minimum, we find that this condition yields the trivial solution $a_2(r) \equiv 0$ (with non-vanishing a_1). Indeed, from equations (32) it is straightforward to see that $a_2(r) \equiv 0$ is a solution of the system. When $\zeta_0 \neq 0$, equations (30) and (31) are coupled, but they still allow the trivial solution $a_2(r) \equiv 0$, which minimizes $|a_2(R)|$, with non-vanishing a_1. The existence of this solution is a remarkable property of this system, and it is due to the fact that the integral in θ on the left-hand side of equation (31) vanishes for $a_2 = 0$ (the integrand becomes odd for parity transformations $\theta \to \pi - \theta$). Hence, if we look for a solution which minimizes the contributions from the $l > 1$ components at the stellar surface, we have to choose the trivial solution $a_2(r) \equiv 0$.

If, instead, we do not require that $a_2(R)$ is minimum, and assign a finite value to the ratio $a_2(R)/a_1(R)$, we find a non-trivial field configuration which is non-symmetric with respect to the equatorial plane. This feature is shown in Fig. 3, where the projection of the field lines in the meridional plane is plotted for $\zeta_0 = 0$ and $a_2(R)/a_1(R)$ equal to 1, 1/2 and 1/4, respectively.

5 THE GENERAL CASE

When all harmonics are taken into account, there exist two distinct classes of solutions: those *symmetric* (with respect to the equatorial plane), with vanishing even-order components ($a_{2l} \equiv 0$), and the *antisymmetric* solutions, with vanishing odd-order components ($a_{2l+1} \equiv 0$). Both solutions satisfy the GS equation (22). Let us consider the symmetric class. When $a_{2l} = 0$, the integrals arising when equation (22) is projected on to the even harmonics, which couple odd and even terms, vanish since the integrands change sign under parity transformations. Therefore, the symmetric solutions can be found by setting $a_{2l} \equiv 0$, projecting equation (22) on to the odd harmonics and solving the resulting equations for a_{2l+1}. Similarly, the integrals in equation (22) projected on to the odd harmonics vanish when $a_{2l+1} = 0$; thus, we can consistently set $a_{2l+1} \equiv 0$, and find the antisymmetric solutions using the same procedure.

In Section 4, we set the value of a_1 at the surface to be 1.93×10^{-3} km and minimized the $l = 2$ contribution. It is clear that, since the $l = 1$ and 2 multipoles belong to different families, any attempt to minimize the relative weight of one with respect to the other leads to the trivial solution. The properties of equation (22) discussed above tell us that if $a_1(R) \neq 0$ we cannot consistently set to zero the remaining odd-order components a_{2l+1}. However, we have the freedom of setting to zero all even terms a_{2l}. Therefore, since we have chosen to minimize the contributions of the $l > 1$ harmonics outside the star, we will focus on the symmetric family of solutions ($a_{2l} \equiv 0$); we will briefly discuss an example belonging to the antisymmetric family in Section 5.4.

5.1 The case with $l = 1$ and 3

We now consider the system of equations including only the $l = 1$ and 3 components. The projected system is

$$\begin{aligned}
&\frac{1}{4\pi}\left(\mathrm{e}^{-\lambda}a_1'' + \mathrm{e}^{-\lambda}\frac{\nu'-\lambda'}{2}a_1' - \frac{2}{r^2}a_1\right)\\
&-\frac{\mathrm{e}^{-\nu}}{4\pi}\int_0^\pi (3/4)\,\zeta_0^2\left(\psi - 3\psi|\psi/\bar{\psi}| + 2\psi^3/\bar{\psi}^2\right)\\
&\times\Theta(|\psi/\bar{\psi}|-1)\sin\theta\,\mathrm{d}\theta\\
&= \left[c_0 - \frac{4}{5}c_1\left(a_1 - \frac{3}{7}a_3\right)\right](\rho + P)r^2,
\end{aligned} \tag{33}$$

$$\begin{aligned}
&\frac{1}{4\pi}\left(\mathrm{e}^{-\lambda}a_3'' + \mathrm{e}^{-\lambda}\frac{\nu'-\lambda'}{2}a_3' - \frac{12}{r^2}a_3\right)\\
&+\frac{\mathrm{e}^{-\nu}}{4\pi}\int_0^\pi (7/48)\,\zeta_0^2\left(\psi - 3\psi|\psi/\bar{\psi}| + 2\psi^3/\bar{\psi}^2\right)\\
&\times\Theta(|\psi/\bar{\psi}|-1)(3 - 15\cos^2\theta)\sin\theta\,\mathrm{d}\theta\\
&= \frac{2}{15}c_1(\rho + P)r^2(a_1 - 4a_3),
\end{aligned} \tag{34}$$

where

$$\psi = \left[-a_1 + \frac{a_3(3 - 15\cos^2\theta)}{2}\right]\sin^2\theta. \tag{35}$$

We again impose regularity at the origin (equation 24), continuity in $r = R$ of a_1, a_1', a_3, a_3' with the vacuum solutions for $a_1(r)$, $a_3(r)$ given by equation (26), and fix $a_1(R) = 1.93 \times 10^{-3}$ km by normalization. For the remaining constraint, we choose the solution that minimizes the absolute value of $a_3(R)$. We find that there is a discrete series of local minima of $|a_3(R)|$, and select among them the absolute minimum.

Fig. 4 shows the profiles of the tetrad field components (see equation 29) obtained by numerically integrating equations (33) and (34), for different values of ζ_0. $B_{(r)}$ is evaluated at $\theta = 0$, while $B_{(\theta)}$, $B_{(\phi)}$ are evaluated at $\theta = \pi/2$. As ζ_0 increases, the magnitude of the toroidal field becomes larger, but the region where it is confined shrinks, as already found in Section 3. The projection of the field

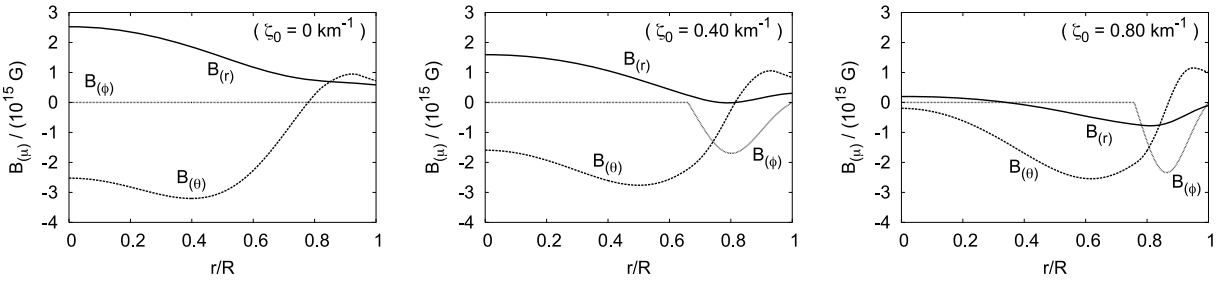

Figure 4. The profiles of the tetrad components of the magnetic field [$B_{(r)}(\theta = 0)$, $B_{(\theta)}(\theta = \pi/2)$, $B_{(\phi)}(\theta = \pi/2)$] are shown for $\zeta_0 = 0$, 0.40 and 0.80 km^{-1}, and $l = 1, 3$.

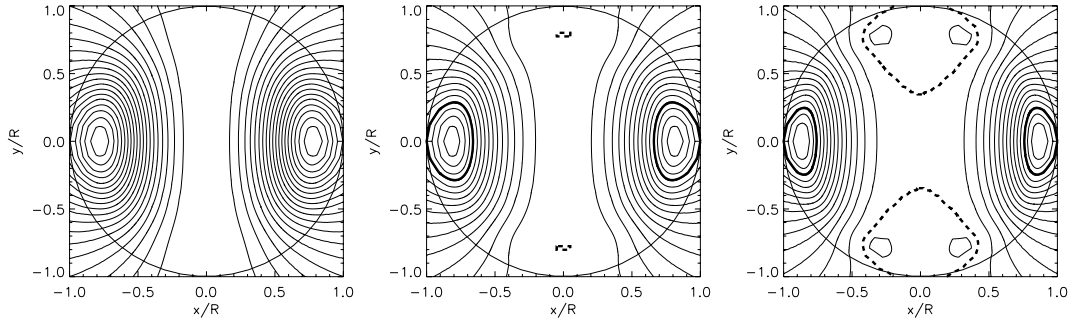

Figure 5. The projection of the field lines in the meridional plane is shown for $\zeta_0 = 0, 0.40, 0.80\,\mathrm{km}^{-1}$, respectively, and $l = 1, 3$. The dashed lines correspond to the $\psi = 0$ surfaces, and the toroidal field is confined within the marked region.

lines in the meridional plane is shown in Fig. 5 for the same values of ζ_0. It shows that, for $\zeta_0 \gtrsim 0.40\,\mathrm{km}^{-1}$, the magnetic field lines lie in disconnected regions, separated by dashed lines in the figure. Inside these regions, the function ψ has opposite sign and no toroidal field is present. A similar phenomenon has been discussed in Colaiuda et al. (2008). As we will see in the next section, the occurrence of these regions is an artefact of the truncation in the harmonic expansion, and disappears as higher-order harmonics are included.

For completeness, we also mention that the solutions corresponding to the local minima of $|a_3(R)|$ different from the absolute minimum correspond to very peculiar field configurations (see Fig. 6). The function ψ has nodes on the equatorial plane, therefore the field lines lie in disconnected regions; for a fixed value of ζ_0, the number of nodes increases as $|a_3(R)|$ increases. These peculiar solutions exist for any value of ζ_0, and appear also when higher-order harmonic components are considered. Thus, they are not artefacts of the l-truncation.

5.2 The case with $l = 1, 3, 5$

We now include the $l = 5$ contribution. The three equations obtained by projecting the GS equation (22) on to $l = 1, 3, 5$ are given in Appendix A. The boundary conditions are essentially the same as in the previous Section; in particular, we look for the absolute minimum of $a_3(R)^2 + a_5(R)^2$, with fixed $a_1(R) = 1.93 \times 10^{-3}$ km.

In Fig. 7, the profiles of the tetrad components of the magnetic field are plotted for values of ζ_0 in the range $0 \leq \zeta_0 \leq 3.00\,\mathrm{km}^{-1}$. Fig. 8 shows the projections of the field lines in the meridional plane corresponding to the same values of ζ_0. Comparing the results with the case $l = 1, 3$, we see that the presence of the harmonic $l = 5$ modifies the magnetic field shape, but most of the features discussed in the previous Section are still present.

An interesting difference is the following. While in the case $l = 1, 3$ for $\zeta_0 \gtrsim 0.40\,\mathrm{km}^{-1}$ we find field configurations which exhibit two disconnected regions where the function ψ has opposite sign and

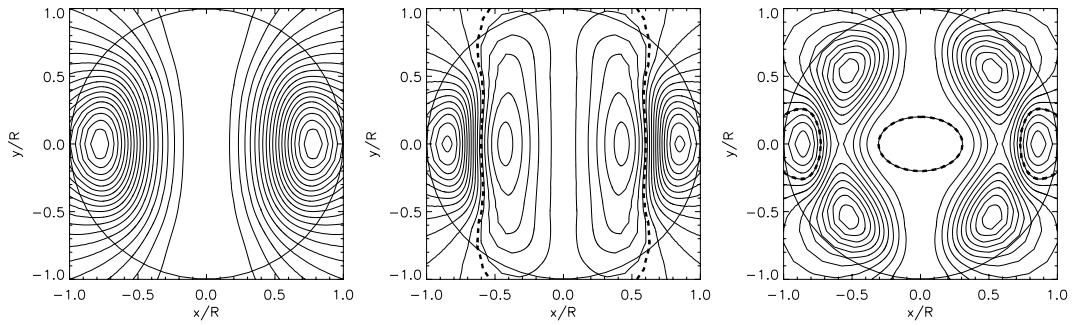

Figure 6. The projection of the field lines in the meridional plane is shown for $\zeta_0 = 0\,\mathrm{km}^{-1}$ and $l = 1, 3$. The left-hand panel refers to the solution corresponding to the absolute minimum of $|a_3(R)/a_1(R)|$; in this solution, ψ has no nodes. The centre and right-hand panels refer to solutions corresponding to relative minima of $|a_3(R)/a_1(R)|$; in these cases, ψ has one and two nodes, respectively. The dashed lines corresponds to the $\psi = 0$ surfaces.

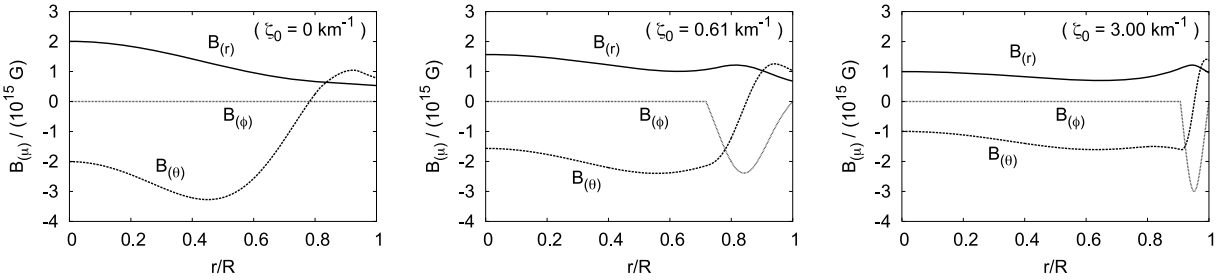

Figure 7. The profiles of the tetrad components of the magnetic field [$B_{(r)}(\theta = 0)$, $B_{(\theta)}(\theta = \pi/2)$, $B_{(\phi)}(\theta = \pi/2)$] for the case including $l = 1, 3, 5$, with $\zeta_0 = 0$, 0.61 and 3.00 km^{-1}.

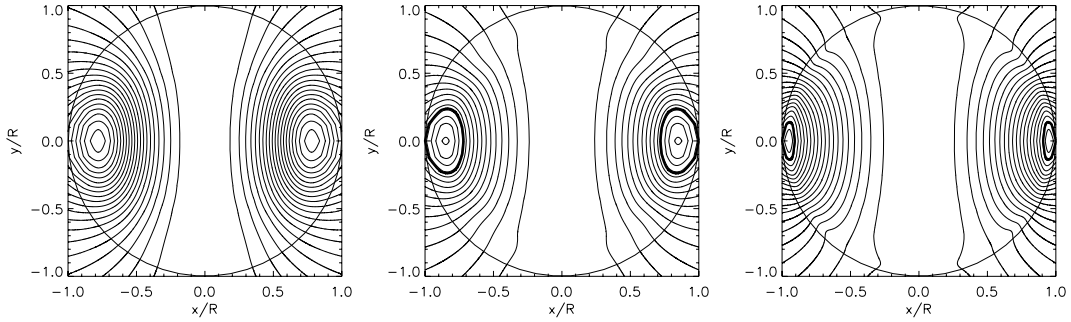

Figure 8. The projection of the field lines in the meridional plane is shown for $\zeta_0 = 0$, 0.61 and 3.00 km^{-1}, respectively, and for $l = 1, 3, 5$. The toroidal field is confined within the marked region.

the magnetic field lines are confined (regions within dashed lines in Fig. 5), this does not occur when the $l = 5$ component is taken into account. This shows that the above feature has to be considered as an artefact of the truncation in the harmonic expansion.

5.3 Higher-order multipoles

Up to now, we have included components with $l < 7$, neglecting the contribution from $l \geq 7$. In order to test the accuracy of this approximation, we have studied the convergence of the harmonic expansion. To this purpose, we have solved the GS equation (22) including odd harmonic components up to $l = 7$, for $\zeta_0 = 0$ and 0.61 km^{-1}, and computed the quantities

$$\Delta^{(5)}(r,\theta) = \left| \frac{\psi_{l\leq 5}(r,\theta) - \psi_{l\leq 3}(r,\theta)}{\bar{\psi}} \right|,$$
$$\Delta^{(7)}(r,\theta) = \left| \frac{\psi_{l\leq 7}(r,\theta) - \psi_{l\leq 5}(r,\theta)}{\bar{\psi}} \right|. \tag{36}$$

These functions are shown in Fig. 9. They are plotted only inside the star since outside they are much smaller. Fig. 9 shows that the error in neglecting $l \geq 7$, quantified by the function $\Delta^{(7)}$, is $\lesssim$2 per cent for $\zeta_0 = 0$ and $\lesssim$4 per cent for $\zeta_0 = 0.61\,\mathrm{km}^{-1}$. Furthermore, a comparison of $\Delta^{(5)}$ and $\Delta^{(7)}$ shows that the harmonic expansion converges.

5.4 An example of antisymmetric solution

Here, we show an example of a solution belonging to the antisymmetric family corresponding to $l = 2, 4$. In Fig. 10, we plot the field lines projected on the meridional plane, for $\zeta_0 = 0$ and 0.30 km^{-1}. We remark that the field lines are antisymmetric with respect to the equatorial plane; as a consequence, the total magnetic helicity is zero (see Section 6). Similar zero-helicity configurations have been considered in Braithwaite (2008a).

6 MAGNETIC HELICITY AND ENERGY

The stationary configurations of magnetized neutron stars which we have found depend on the value of the free parameter ζ_0, i.e. on the ratio between the toroidal and the poloidal components of the magnetic field. In this section, we provide an argument to assign a value to ζ_0. Furthermore, we compute the magnetic energy of the system to compare the contributions from poloidal and toroidal fields.

The total energy of the system (the star, the magnetic field and the gravitational field) can be determined by looking at the far-field limit ($r \to \infty$) of the space–time metric (Misner, Thorne & Wheeler 1973; Thorne 1980). Following Colaiuda et al. (2008) and Ioka & Sasaki (2004), we write the perturbed metric as

$$\begin{aligned} \mathrm{d}s^2 = &-\mathrm{e}^{\nu}\Big[1 + 2h(r,\theta)\Big]\mathrm{d}t^2 + \mathrm{e}^{\lambda}\left[1 + \frac{2\mathrm{e}^{\lambda}}{r}m(r,\theta)\right]\mathrm{d}r^2 \\ &+ r^2\Big[1 + 2k(r,\theta)\Big](\mathrm{d}\theta^2 + \sin^2\theta\,\mathrm{d}\phi^2) \\ &+ 2i(r,\theta)\,\mathrm{d}t\,\mathrm{d}r + 2v(r,\theta)\,\mathrm{d}t\,\mathrm{d}\phi + 2w(r,\theta)\,\mathrm{d}r\,\mathrm{d}\phi, \end{aligned} \tag{37}$$

where, in particular, $m(r,\theta) = \sum_l m_l(r) P_l(\cos\theta)$. The total mass–energy of the system is

$$E = M + \delta M, \tag{38}$$

where M is the gravitational mass of the unperturbed star and

$$\delta M = \lim_{r\to\infty} m_0(r)\,. \tag{39}$$

In Appendix B, we discuss the equations which allow to determine E. We remark that δM includes different contributions, due to magnetic energy, deformation energy, etc.

In order to evaluate the magnetic contribution to E, it is convenient to use the Komar–Tolman formula (see e.g. Straumann 2004,

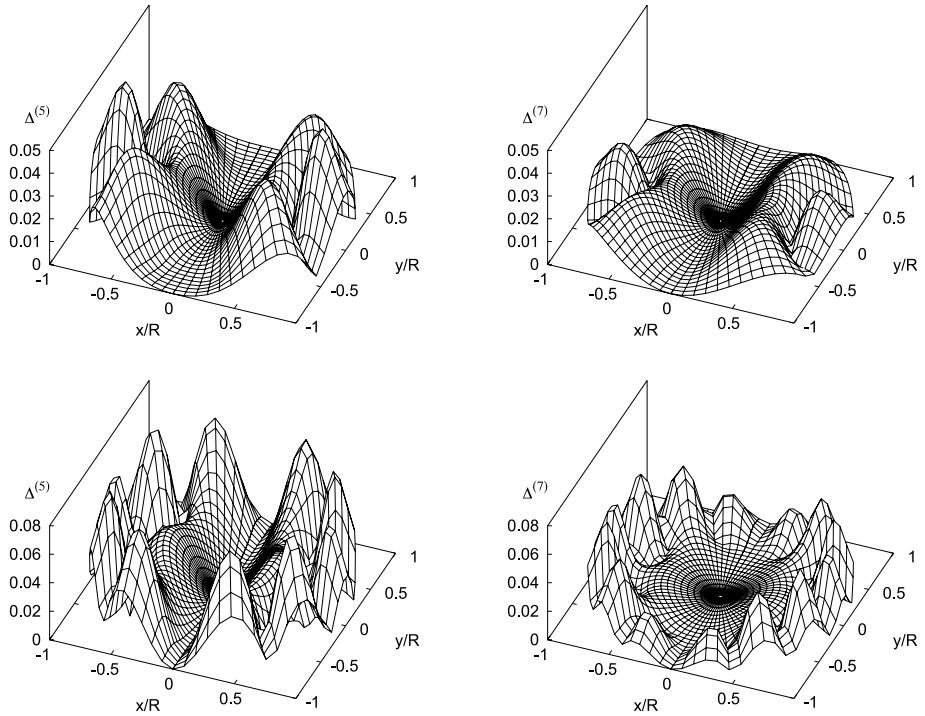

Figure 9. The functions $\Delta^{(5)}$ (left-hand panels) and $\Delta^{(7)}$ (right-hand panels) are shown for $\zeta_0 = 0$ (upper panels) and $\zeta_0 = 0.61\,\mathrm{km}^{-1}$ (lower panels) in the meridional plane for $0 \leq r \leq R$.

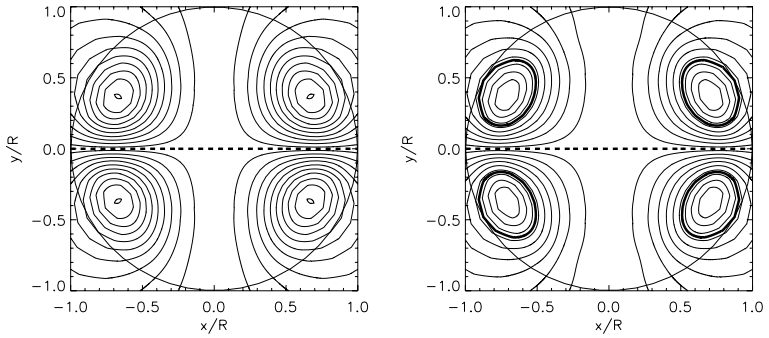

Figure 10. The projection of the field lines in the meridional plane is shown for $\zeta_0 = 0$ and $0.30\,\mathrm{km}^{-1}$, respectively, and for $l = 2$, 4. The dashed line corresponds to $\psi = 0$; the toroidal field is confined within the marked region.

chapter 4) for the total energy:

$$E = 2\int_V \left(\boldsymbol{T}_{\mu\nu} - \frac{1}{2}T\boldsymbol{g}_{\mu\nu}\right)\eta^\mu n^\nu \,\mathrm{d}V, \tag{40}$$

where V is the three-surface at constant time, η^μ is the time-like Killing vector, n^μ is the normalized, future directed normal to V; the magnetic contribution comes from the stress–energy tensor of the electromagnetic field, $\boldsymbol{T}^{\mu\nu}_{\mathrm{em}}$ (3), i.e.

$$\begin{aligned} E_{\mathrm{m}} &= 2\int_V \left(\boldsymbol{T}^{\mathrm{em}}_{\mu\nu} - \frac{1}{2}\boldsymbol{T}^{\mathrm{em}}\boldsymbol{g}_{\mu\nu}\right)\eta^\mu n^\nu \,\mathrm{d}V \\ &= \frac{1}{2}\int_0^\infty r^2 \mathrm{e}^{\frac{\lambda+\nu}{2}}\,\mathrm{d}r \int_0^\pi \sin\theta\; B^2\,\mathrm{d}\theta\,. \end{aligned} \tag{41}$$

The total (integrated) magnetic helicity H_{m} of the field configuration is

$$H_{\mathrm{m}} = \int \mathrm{d}^3x\sqrt{-g}H^0_{\mathrm{m}}, \tag{42}$$

where H^0_{m} is the t-component of the magnetic helicity four-current, defined as

$$H^\alpha_{\mathrm{m}} = \frac{1}{2}\epsilon^{\alpha\beta\gamma\delta}F_{\gamma\delta}A_\beta. \tag{43}$$

Explicitly, we have

$$H_{\mathrm{m}} = -2\pi\int_0^R \mathrm{d}r\int_0^\pi (A_r\psi_{,\theta} - \psi A_{r,\theta})\,\mathrm{d}\theta, \tag{44}$$

where

$$\begin{aligned} \psi A_{r,\theta} &= \frac{\mathrm{e}^{\frac{\lambda-\nu}{2}}}{\sin\theta}\psi^2\zeta_0\left(|\psi/\bar{\psi}| - 1\right)\Theta(|\psi/\bar{\psi}| - 1), \\ \psi_{,\theta}A_r &= \psi_{,\theta}\mathrm{e}^{\frac{\lambda-\nu}{2}}\zeta_0\int_0^\theta \frac{\psi}{\sin\theta'}\left(|\psi/\bar{\psi}| - 1\right) \\ &\quad\times\Theta(|\psi/\bar{\psi}| - 1)\,\mathrm{d}\theta'. \end{aligned} \tag{45}$$

The functional dependence of H_{m} on the potential of the toroidal field, A_r (see equation 44), shows that regions of space where the toroidal field vanishes do not contribute to the magnetic helicity.

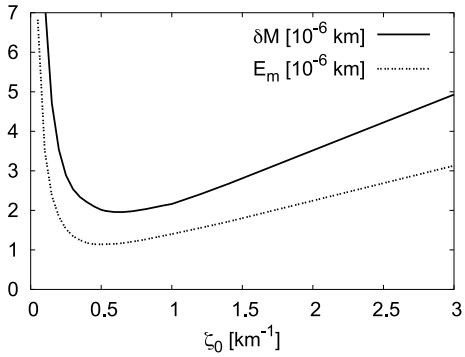

Figure 11. The functions δM and $E_{\rm m}$ are plotted as functions of ζ_0, for $l = 1, 3, 5$ and $H_{\rm m} = 1.75 \times 10^{-6}\,{\rm km}^2$.

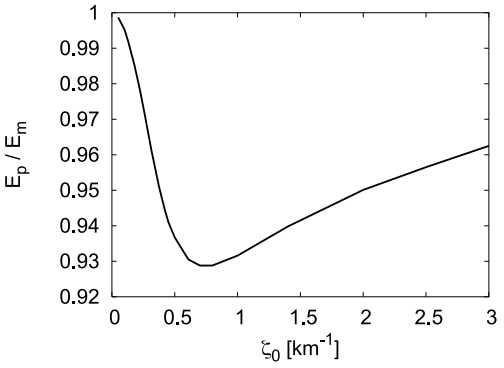

Figure 12. The ratio $E_{\rm p}/E_{\rm m}$ is shown as a function of ζ_0, for $l = 1, 3, 5$.

In ideal MHD, the magnetic helicity is a conserved quantity (Bekenstein 1987; Braithwaite & Spruit 2006). Thus, if we consider magnetic field configurations having the same value of the magnetic helicity and different energies, the lowest energy configuration is energetically favoured.

In Fig. 11, we plot δM and $E_{\rm m}$ as functions of ζ_0, for a fixed helicity $H_{\rm m} = 1.75 \times 10^{-6}\,{\rm km}^2$. δM, and consequently the total energy, has a minimum at $\zeta_0 = 0.61\,{\rm km}^{-1}$. A fixed value of $H_{\rm m}$ corresponds, for any assigned value of ζ_0, to a different normalization constant $B_{\rm pole}$. Since δM, $H_{\rm m}$ and $E_{\rm m}$ have the same quadratic dependence on the magnetic field normalization, this means that if we change $H_{\rm m}$ the plots of δM and $E_{\rm m}$ as functions of ζ_0 are simply rescaled with respect to that shown in Fig. 11. Consequently, for any fixed value of $H_{\rm m}$ the position of the minimum of the total energy is the same as that shown in Fig. 11. We conclude that the configuration with $\zeta_0 \simeq 0.61\,{\rm km}^{-1}$ is energetically favoured. This configuration is shown, among others, in Figs 7 and 8. From Fig. 11, we also see that the contribution of the magnetic energy to δM is of the order of ∼50–70 per cent.

In Fig. 12, we show the ratio of poloidal to total magnetic field energy, $E_{\rm p}/E_{\rm m}$, as a function of ζ_0, for the configurations ($l =$ 1, 3, 5) studied in this paper. This plot is interesting because the relative weight of the poloidal and the toroidal components of the field significantly affects many astrophysical processes involving magnetars, like magnetar activity (Woods & Thompson 2006), their thermal evolution (Pons, Miralles & Geppert 2008), their gravitational wave emission (Cutler 2002). It should be mentioned that the surface poloidal field is inferred from spin-down measurements which, however, provide no hint about the toroidal field hidden inside the star. We find that for $\zeta_0 = 0.61\,{\rm km}^{-1}$, $E_{\rm p}/E_{\rm m} \simeq 0.93$.

In a recent paper (Braithwaite 2008b), the stability of magnetic field configurations of compact stars has been studied in the context of Newtonian gravity, and by assuming a polytropic EOS. It has been found that axisymmetric configurations are stable when $0.01 \lesssim E_{\rm p}/E_{\rm m} \lesssim 0.8$. Our configurations are outside this range, i.e. $E_{\rm p}/E_{\rm m} > 0.9$. This difference may be attributed to several reasons: our models are computed in the framework of general relativity, we use a more realistic EOS, we choose a particular function $\zeta(\psi)$, which is linear in $(|\psi/\bar{\psi}| - 1)$ (see equation 10). A different power-law dependence may lead to a different contribution of the toroidal field. In any case, we observe a tendency in favour of models with predominant poloidal fields when using arguments of minimum energy, and do not think that other functional forms of ζ may result in configurations with most of the energy stored in the toroidal field. This issue deserves further investigations.

7 DISCUSSION AND CONCLUSIONS

In this paper, we find a twisted torus family of solutions in the framework of general relativity. The toroidal component of the magnetic field vanishes outside the star: neither discontinuities (associated to surface currents) nor the vanishing of the total magnetic field outside the star has been imposed; this is an improvement with respect to previous works (Ioka & Sasaki 2004; Colaiuda et al. 2008; Haskell et al. 2008). It should be stressed that twisted torus configurations have been found to emerge as a final outcome of Newtonian MHD simulations with generic initial conditions (Braithwaite & Spruit 2004; Braithwaite & Nordlund 2006; Braithwaite & Spruit 2006).

In order to have a twisted torus configuration, there must be a non-linear relation between toroidal and poloidal fields, leading to couplings between different multipoles. We have investigated the contributions of different harmonics, and constructed equilibrium configurations with $1 \leq l \leq 5$. In order to fix the boundary conditions, we imposed that outside the star the dipolar component dominates, and minimized the $l > 1$ contributions which, however, remain non-negligible. We find that there exist two particular, independent classes of solutions: those *symmetric* (with respect to the equatorial plane), in which all even-order components vanish ($a_{2l} \equiv 0$), and the *antisymmetric* solutions, characterized by the vanishing of odd components ($a_{2l+1} \equiv 0$). The latter have zero helicity by definition, therefore any solution minimizing energy at fixed helicity has a vanishing antisymmetric component.

Our models also depend on a parameter, ζ_0, which determines the ratio between toroidal and poloidal fields ($\approx \zeta_0 R$), and the length-scale of the region where the toroidal field is confined ($\propto \zeta_0^{-1}$). As ζ_0 increases, the amplitude of the toroidal field grows, but the region where it is confined shrinks. This parameter can be estimated by minimizing the total energy at fixed magnetic helicity. We find that, for our neutron star model (EOS APR2, $M = 1.4\,{\rm M}_\odot$), this minimum occurs at $\zeta_0 = 0.61\,{\rm km}^{-1}$. Therefore, we expect that in the early evolution of a strongly magnetized (fluid) neutron star the natural final outcome after MHD equilibrium is established is twisted torus configurations with geometries similar to our solutions.

Finally, we have computed the magnetic energy associated to the poloidal and toroidal fields. We find that, although the amplitudes of both fields are of the same order of magnitude, and the toroidal field in the interior can be larger than the poloidal field at the surface (for instance, it is 2–3 times larger if $\zeta_0 = 0.61\,{\rm km}^{-1}$), the

contribution of the toroidal field to the total magnetic energy is $\lesssim$10 per cent, because this field is non-vanishing only in a finite region of the star. As mentioned in Section 6, a different power-law dependence of the function $\zeta(\psi)$ on $(|\psi/\bar{\psi}|-1)$ may lead to a different contribution of the toroidal field, and we plan to investigate this issue in a forthcoming paper.

Note: After our paper has been submitted and sent to the arXiv, a paper has appeared (Lander & Jones 2009) where a model of magnetar with twisted torus magnetic field configuration is developed in the Newtonian framework. The results of Lander & Jones (2009) are in agreement with ours, in that they find the toroidal field to be bounded to less than 7 per cent of the total magnetic field.

ACKNOWLEDGMENTS

This work was partially supported by the Spanish grant AYA 2007-67626-C03-02 and COMPSTAR, an ESF Research Networking Programme.

REFERENCES

Aguilera D. N., Pons J. A., Miralles J. A., 2008, A&A, 486, 255
Akmal A., Pandharipande V. R., Ravenhall D. G., 1998, Phys. Rev. C, 58, 1804
Bekenstein J. D., 1987, ApJ, 319, 207
Benhar O., Ferrari V., Gualtieri L., 2004, Phys. Rev. D, 70, 124015
Braithwaite J., Nordlund Å., 2006, A&A, 450, 1077
Braithwaite J., Spruit H. C., 2004, Nat, 431, 819
Braithwaite J., Spruit H. C., 2006, A&A, 450, 1097
Braithwaite J., 2008a, MNRAS, 386, 1947
Braithwaite J., 2008b, MNRAS, in press (arXiv:0810.1049)
Colaiuda A., Ferrari V., Gualtieri L., Pons J. A., 2008, MNRAS, 385, 2080
Cutler C., 2002, Phys. Rev. D, 66, 084025
Duncan R. C., Thompson C., 1992, ApJ, 392, L9
Geppert U., Rheinhardt M., 2006, A&A, 456, 639
Haskell B., Samuelsson L., Glampedakis K., Andersson N., 2008, MNRAS, 385, 531
Ioka K., Sasaki M., 2004, ApJ, 600, 296
Konno K., Obata T., Kojima Y., 1999, A&A, 352, 211
Lander S. K., Jones D. I., 2009, MNRAS, 395, 2162
Lyutikov M., 2006, MNRAS, 367, 1594
Misner C. W., Thorne K. S., Wheeler J. A., 1973, Gravitation. W.H. Freeman & co., New York
Pavan L., Turolla R., Zane S., Nobili A., 2009, MNRAS, 395, 753
Pons J. A., Geppert U., 2007, A&A, 470, 303
Pons J. A., Miralles J. A., Geppert U., 2008, A&A, 496, 207
Prendergast K. H., 1956, ApJ, 123, 498
Straumann N., 2004, General Relativity. Springer-Verlag, Berlin
Thorne K. S., 1980, Rev. Mod. Phys., 52, 299
Woods P. M., Thompson C., 2006, in Lewin W., van der Klis M., eds, Compact Stellar X-Ray Sources, Cambridge Astrophys. Ser. 39. Cambridge Univ. Press, Cambridge, p. 547
Yoshida S., Eriguchi Y., 2006, ApJS, 164, 156
Yoshida S., Yoshida S., Eriguchi Y., 2006, ApJ, 651, 462

APPENDIX A: GS EQUATION FOR THE CASE WITH $l = 1, 3, 5$

If we include the $l = 1, 3, 5$ components, the GS equation (22) projected onto the harmonics $l = 1, 3, 5$ gives the following system:

$$\frac{1}{4\pi}\left(\mathrm{e}^{-\lambda}a_1'' + \mathrm{e}^{-\lambda}\frac{\nu'-\lambda'}{2}a_1' - \frac{2}{r^2}a_1\right) - \frac{\mathrm{e}^{-\nu}}{4\pi}\int_0^\pi (3/4)\,\zeta_0^2\left(\psi - 3\psi|\psi/\bar{\psi}| + 2\psi^3/\bar{\psi}^2\right) \times \Theta(|\psi/\bar{\psi}|-1)\sin\theta\,\mathrm{d}\theta = \left[c_0 - \frac{4}{5}c_1\left(a_1 - \frac{3}{7}a_3\right)\right](\rho+P)r^2\,, \tag{A1}$$

$$\frac{1}{4\pi}\left(\mathrm{e}^{-\lambda}a_3'' + \mathrm{e}^{-\lambda}\frac{\nu'-\lambda'}{2}a_3' - \frac{12}{r^2}a_3\right) + \frac{\mathrm{e}^{-\nu}}{4\pi}\int_0^\pi (7/48)\,\zeta_0^2\left(\psi - 3\psi|\psi/\bar{\psi}| + 2\psi^3/\bar{\psi}^2\right) \times \Theta(|\psi/\bar{\psi}|-1)(3-15\cos^2\theta)\sin\theta\,\mathrm{d}\theta = c_1(\rho+P)r^2\left(\frac{2}{15}a_1 - \frac{8}{15}a_3 + \frac{10}{33}a_5\right), \tag{A2}$$

$$\frac{1}{4\pi}\left(\mathrm{e}^{-\lambda}a_5'' + \mathrm{e}^{-\lambda}\frac{\nu'-\lambda'}{2}a_5' - \frac{30}{r^2}a_5\right) + \frac{\mathrm{e}^{-\nu}}{4\pi}\int_0^\pi (11/60)\,\zeta_0^2\left(\psi - 3\psi|\psi/\bar{\psi}| + 2\psi^3/\bar{\psi}^2\right) \times \Theta(|\psi/\bar{\psi}|-1)\frac{(-315\cos^4\theta + 210\cos^2\theta - 15)}{8}\sin\theta\,\mathrm{d}\theta = c_1(\rho+P)r^2\left(\frac{4}{21}a_3 - \frac{20}{39}a_5\right), \tag{A3}$$

where

$$\psi = \left[-a_1 + \frac{a_3(3-15\cos^2\theta)}{2} + \frac{a_5(-315\cos^4\theta + 210\cos^2\theta - 15)}{8}\right]\sin^2\theta.$$

APPENDIX B: THE ENERGY OF THE SYSTEM

The perturbation of the total energy of the system can be determined from the far-field limit of the space–time metric (Misner et al. 1973; Thorne 1980; Ioka & Sasaki 2004):

$$\delta M = \lim_{r\to\infty} m_0(r), \tag{B1}$$

where the perturbed metric is given by equation (37). The functions $h(r,\theta)$ and $m(r,\theta)$ are

$$h(r,\theta) = \sum_l h_l(r)P_l(\cos\theta),$$
$$m(r,\theta) = \sum_l m_l(r)P_l(\cos\theta). \tag{B2}$$

The perturbed Einstein equations ($[tt]$ and $[rr]$ components), projected onto $l = 0$, allow to determine the quantity $m_0(r)$:

$$m_0' - 4\pi r^2\frac{\rho'}{P'}\delta p_0 = \frac{1}{3}(a_1')^2\mathrm{e}^{-\lambda} + \frac{6}{7}(a_3')^2\mathrm{e}^{-\lambda} + \frac{15}{11}(a_5')^2\mathrm{e}^{-\lambda} + \frac{2}{3r^2}a_1^2 + \frac{72}{7r^2}a_3^2 + \frac{450}{11r^2}a_5^2 + \frac{\mathrm{e}^{-\nu}}{4}\left[\int_0^\pi \zeta_0^2\left(|\psi/\bar{\psi}|-1\right)^2\Theta(|\psi/\bar{\psi}|-1)\frac{\psi^2}{\sin\theta}\mathrm{d}\theta\right],$$

$$
\begin{aligned}
&h_0' - \mathrm{e}^{2\lambda} m_0 \left(\frac{1}{r^2} + 8\pi P\right) - 4\pi r \mathrm{e}^{\lambda} \delta p_0 \\
&\quad = \frac{1}{3r}(a_1')^2 + \frac{6}{7r}(a_3')^2 + \frac{15}{11r}(a_5')^2 - \frac{2\mathrm{e}^{\lambda}}{3r^3}a_1^2 \\
&\quad - \frac{72\mathrm{e}^{\lambda}}{7r^3}a_3^2 - \frac{450\mathrm{e}^{\lambda}}{11r^3}a_5^2 \\
&\quad + \frac{\mathrm{e}^{\lambda-\nu}}{4r}\left[\int_0^{\pi} \zeta_0^2 \left(|\psi/\bar{\psi}| - 1\right)^2 \Theta(|\psi/\bar{\psi}| - 1)\frac{\psi^2}{\sin\theta}\,\mathrm{d}\theta\right], \qquad \text{(B3)}
\end{aligned}
$$

where δp_0 is the $l = 0$ component of the pressure perturbation (and vanishes outside the star) and $\psi = \sin\theta \sum_{l=1,3,5} a_l P_{l,\theta}$. Using the relation (arising from $T^{rv}_{\ ;v} = 0$)

$$
\begin{aligned}
\delta p_0' = &-\frac{\nu'}{2}\left(\frac{\rho'}{P'} + 1\right)\delta p_0 - (\rho + P)h_0' \\
&- \frac{2}{3}a_1'(\rho + P)\left[c_0 - \frac{4}{5}c_1\left(a_1 - \frac{3}{7}a_3\right)\right] \\
&- \frac{12}{7}a_3'(\rho + P)c_1\left(\frac{2}{15}a_1 - \frac{8}{15}a_3 + \frac{10}{33}a_5\right) \\
&- \frac{10}{11}a_5'(\rho + P)c_1\left(\frac{4}{21}a_3 - \frac{20}{39}a_5\right), \qquad \text{(B4)}
\end{aligned}
$$

equations (B3) can be rearranged in the form

$$
\begin{aligned}
&m_0' - 4\pi r^2 \frac{\rho'}{P'}\delta p_0 = \frac{1}{3}(a_1')^2 \mathrm{e}^{-\lambda} + \frac{6}{7}(a_3')^2 \mathrm{e}^{-\lambda} + \frac{15}{11}(a_5')^2 \mathrm{e}^{-\lambda} \\
&\quad + \frac{2}{3r^2}a_1^2 + \frac{72}{7r^2}a_3^2 + \frac{450}{11r^2}a_5^2 \\
&\quad + \frac{\mathrm{e}^{-\nu}}{4}\left[\int_0^{\pi} \zeta_0^2 \left(|\psi/\bar{\psi}| - 1\right)^2 \Theta(|\psi/\bar{\psi}| - 1)\frac{\psi^2}{\sin\theta}\mathrm{d}\theta\right], \\
&\delta p_0' + \left[\frac{\nu'}{2}\left(\frac{\rho'}{P'} + 1\right) + 4\pi r \mathrm{e}^{\lambda}(\rho + P)\right]\delta p_0 \\
&\quad + \mathrm{e}^{2\lambda} m_0 (\rho + P)\left(\frac{1}{r^2} + 8\pi P\right) \\
&\quad = (\rho + P)\left\{ - \frac{2}{3}a_1'\left[c_0 - \frac{4}{5}c_1\left(a_1 - \frac{3}{7}a_3\right)\right]\right. \\
&\quad - \frac{12}{7}a_3' c_1\left(\frac{2}{15}a_1 - \frac{8}{15}a_3 + \frac{10}{33}a_5\right) \\
&\quad - \frac{10}{11}a_5' c_1\left(\frac{4}{21}a_3 - \frac{20}{39}a_5\right) - \frac{1}{3r}(a_1')^2 - \frac{6}{7r}(a_3')^2 \\
&\quad - \frac{15}{11r}(a_5')^2 + \frac{2\mathrm{e}^{\lambda}}{3r^3}a_1^2 + \frac{72\mathrm{e}^{\lambda}}{7r^3}a_3^2 + \frac{450\mathrm{e}^{\lambda}}{11r^3}a_5^2 \\
&\quad \left. - \frac{\mathrm{e}^{\lambda-\nu}}{4r}\left[\int_0^{\pi} \zeta_0^2 \left(|\psi/\bar{\psi}| - 1\right)^2 \Theta(|\psi/\bar{\psi}| - 1)\frac{\psi^2}{\sin\theta}\mathrm{d}\theta\right]\right\}. \qquad \text{(B5)}
\end{aligned}
$$

By imposing a regular behaviour at $r \simeq 0$, we find

$$
m_0(r \to 0) = Ar^3, \quad \delta p_0(r \to 0) = Cr^2, \qquad \text{(B6)}
$$

where

$$
\begin{aligned}
C &= -\frac{2(P_c + \rho_c)\left(\alpha_1^2 + \alpha_1 c_0\right)}{3 + 4\pi\left(r^2 \frac{\mathrm{d}\rho}{\mathrm{d}P}\right)_c P_c}, \\
A &= \frac{1}{3}\left[2\alpha_1^2 + 4\pi C\left(r^2 \frac{\mathrm{d}\rho}{\mathrm{d}P}\right)_c\right]. \qquad \text{(B7)}
\end{aligned}
$$

The subscript c means that the quantity is evaluated at $r \to 0$. We remark that the solution of (B5) does not depend on new arbitrary constants. Outside the star, the equation for m_0 reduces to

$$
\begin{aligned}
m_0' = &\left[\frac{1}{3}(a_1')^2 + \frac{6}{7}(a_3')^2 + \frac{15}{11}(a_5')^2\right]\left(1 - \frac{2M}{r}\right) \\
&+ \frac{2}{3r^2}a_1^2 + \frac{72}{7r^2}a_3^2 + \frac{450}{11r^2}a_5^2. \qquad \text{(B8)}
\end{aligned}
$$

Solving (B5) and (B8), we find δM from (B1).

This paper has been typeset from a TEX/LATEX file prepared by the author.